On Volkov's Momentum-Integral Formulation of Viscous and Thermal Boundary Layers for Flow over a Flat Plate

Charles J. Davis* and Joseph Majdalani†
Auburn University, Auburn, AL 36849

Comparisons between the classical Kármán–Pohlhausen (KP) momentum-integral formulation and Volkov's refined integral approach are presented for flow over an isothermal flat plate. The study examines the extent to which predictive accuracy depends on the structure of the integral framework versus the fidelity of the assumed nearfield velocity and temperature profiles. In the traditional KP method, wall shear stress and surface heat flux enter explicitly through velocity and temperature gradients evaluated at the wall, thus rendering the solution sensitive to the local behavior of low-order polynomial approximations. Volkov's refinement circumvents this dependence by replacing the wall-gradient contribution with equivalent integral expressions derived directly from the boundary-layer equations, thereby shifting emphasis from localized derivative evaluations to global integral properties that are more forgiving of the imprecisions introduced by the assumed profiles. To assess the relative merits of both formulations, first-, second-, third-, and fourth-order Pohlhausen polynomials, along with the optimized MX4 velocity profile, are systematically implemented within hydrodynamic and thermal integral analyses. Closed-form expressions are derived for the boundary-layer thickness, displacement and momentum thicknesses, skin-friction coefficient, and average Nusselt number. These predictions are evaluated against the Blasius similarity solution and established flat-plate heat-transfer correlations to quantify deviations attributable to polynomial order and integral structure. The results indicate that Volkov's refinement yields appreciable improvements in wall-shear and heat-transfer predictions when lower-order approximations are employed, namely, by substantially reducing the solution sensitivity to near-wall inaccuracies. However, when paired with optimized velocity representations that closely emulate the Blasius profile, the classical KP formulation still achieves the highest accuracy.

I. Introduction

Integral methods provide a practical analytical avenue for estimating boundary-layer properties without solving the full Navier–Stokes equations. By transforming the conservation principles into an integral form, these methods allow for the semi-analytical evaluation of fundamental flow quantities while retaining the dominant physical characteristics of the flow motion. As a result, integral approaches remain valuable both as efficient engineering design tools and as platforms for assessing the effect of assumed nearfield velocity and temperature distributions on boundary-layer development. More specifically, the implementation of boundary-layer theory in integral form enables us to gain essential physical insights into skin friction, drag, and convective heat transfer behavior, particularly, in applications ranging from airfoils to thermal process equipment and microfluidic devices [1].

Following Blasius' pioneering 1908 similarity solution for laminar flow over a flat plate, several approximations have been advanced to simplify boundary-layer analysis while retaining varying degrees of predictive accuracy [2]. Among these, the classical von Kármán integral method has long been used to estimate hydrodynamic and thermal boundary-layer characteristics [3]. The method is derived directly from the momentum and energy integral equations and yields closed-form analytical expressions when combined with assumed polynomial profiles, such as those postulated by Pohlhausen [4] for the nearfield velocity. The adaptability of the so-called Kármán–Pohlhausen (KP) approach across a broad range of Reynolds numbers has indeed contributed to its widespread adoption in both instructional [1, 5] and applied contexts [6–8].

Improvements to the classical integral KP approach for both nearfield velocity and temperature fields are often discussed [9]. Pohlhausen [4] provides widely adopted polynomial approximations for the nearfield velocity and temperature profiles, while subsequent refinements, such as those by Volkov [10] and the MX4 polynomial by Majdalani and Xuan [6], have been shown to improve the accuracy of the KP method. Volkov's refinement, which is elegantly described by Pitts and Griggs [9], seeks to advance the KP approach by replacing the wall-derivative term in the hydrodynamic integral equation with an equivalent integral representation that reduces the method's sensitivity in the near-wall region [10]. To date, however, systematic extensions of Volkov's approach to thermal boundary-layer

*Undergraduate Research Assistant, Department of Aerospace Engineering, AIAA University Student Member 1840790.
†Professor and Francis Chair, Department of Aerospace Engineering, AIAA Lifetime Fellow 199546.

analysis remain limited, and direct comparisons between classical KP and Volkov-type formulations in hydrodynamic and thermal analysis problems remain largely unexplored. For this reason, the present work will focus on providing a thorough assessment of the the classical KP and Volkov approaches by comparing their results for the canonical problem of incompressible flow over a flat plate using self-similar velocity and temperature fields.

Despite its utility, the classical KP formulation introduces wall shear stress and surface heat flux explicitly through velocity and temperature gradients that are evaluated at the wall [9]. As such, the predictive accuracy of the method becomes strongly dependent on the near-wall behavior of the nearfield velocity profiles, whose precise construction becomes quite essential. When lower-order polynomial approximations are employed to represent the nearfield, such as those devised by Pohlhausen [4], small changes in the derivative at the wall can produce disproportionate deviations in the approximated skin friction and heat transfer properties. In principle, Volkov's formulation modifies the classical integral framework by replacing the explicit wall-gradient terms with integral expressions that tend to reduce the method's reliance on local derivative evaluations in favor of global integral properties [10].

The present study extends Volkov's methodology to thermal boundary-layer analysis and provides a direct analytical comparison between the classical KP method and Volkov's formulation for steady, incompressible, laminar flow over a flat plate. In this effort, the standard Pohlhausen polynomials as well as the improved MX4 polynomial representation of the nearfield velocity will be methodically implemented within each framework to evaluate the fundamental boundary-layer properties, such as the disturbance thickness, skin-friction coefficient, and average Nusselt number. By systematically examining the effect of varying the polynomial order and formulation structure, the relative sensitivity and predictive capability of the two integral methods will be thoroughly assessed and discussed.

II. Hydrodynamic Analysis

In this section, the hydrodynamic analysis of steady, incompressible, viscous flow over a flat plate is developed within the classical boundary-layer framework. The von Kármán momentum-integral method is first employed to obtain analytical expressions for the boundary-layer thickness and local skin-friction coefficient as functions of the local Reynolds number. The Volkov refinement to the integral formulation is then applied to derive corresponding relations. The resulting predictions are subsequently compared with the Blasius similarity solution in order to assess the relative performance of the two integral approaches over the laminar flat-plate regime.

A. Flat-Plate Configuration

The flow configuration that we consider is illustrated in Fig. 1. The incoming flow is taken to be uniform with constant velocity U_∞. As the fluid progresses downstream along the plate, viscous effects within the near-wall region generate a wall shear stress, τ_w, at $y = 0$. At any streamwise location x, the nearfield velocity distribution $u(y)$ evolves from zero at the wall, in adherence with the no-slip physical requirement, to the free stream value, which occurs at the outer edge of the boundary layer.

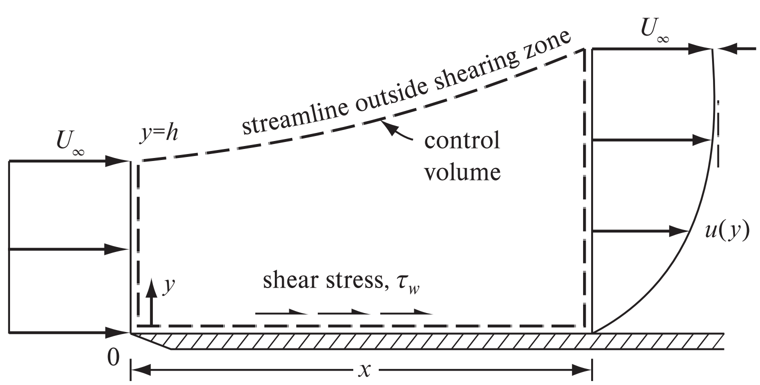

Fig. 1. Control volume used in the canonical analysis of the incompressible flow motion over a flat plate.

B. Von Kármán's Classical Approach

Rather than solving the boundary-layer equations directly, the von Kármán method applies an integral momentum balance across the developing viscous region. To support this formulation, the velocity and wall-normal coordinate are expressed in nondimensional form as $F = u/U_\infty$ and $\eta = y/\delta$. The velocity profile can then be represented as a piecewise function, namely,

$$\frac{u}{U_\infty} = \begin{cases} F(\eta); & 0 \leq \eta \leq 1, \\ 1; & 1 < \eta < \infty. \end{cases} \tag{1}$$

This construction ensures that the freestream condition is satisfied outside the boundary layer. Moreover, it confines the velocity deficit to the finite interval $0 \leq \eta \leq 1$, allowing integrals that are formally written to infinity to be evaluated using only the assumed profile function. For steady, two dimensional flow, the momentum integral equation for a flat plate can be written as

$$\frac{\tau_w}{\rho} = \frac{\partial}{\partial x}(U_\infty^2 \theta) + U_\infty \frac{\partial U_\infty}{\partial x}\delta^*, \tag{2}$$

where θ and δ^* denote the momentum and displacement thicknesses, respectively. These integral measures describe the cumulative effect of the boundary layer on the outer inviscid stream: δ^* represents the apparent displacement of streamlines, while θ quantifies the associated reduction in momentum flux. They are formally given by

$$\theta = \int_0^\delta \frac{u}{U_\infty}\left(1 - \frac{u}{U_\infty}\right) \mathrm{d}y = \delta \int_0^1 F(\eta)[1 - F(\eta)]\, \mathrm{d}\eta \quad \text{and} \quad \delta^* = \int_0^\delta \left(1 - \frac{u}{U_\infty}\right) \mathrm{d}y = \delta \int_0^1 [1 - F(\eta)]\, \mathrm{d}\eta. \tag{3}$$

This transformation confines the streamwise development to $\delta(x)$, while the assumed profile contributes only through constant integral coefficients. At zero angle of incidence, since the streamwise pressure gradient vanishes and the freestream velocity, U_∞, remains invariant, Eq. (2) can be further simplified into:

$$\tau_w = \rho U_\infty^2 \theta^* \frac{\mathrm{d}\delta}{\mathrm{d}x}; \quad \theta^* \equiv \frac{\theta}{\delta}, \tag{4}$$

where θ^* denotes the non-dimensional momentum thickness, a pure constant that depends entirely on the assumed velocity profile $F(\eta)$. This expression provides the direct connection between the wall shear stress and the rate at which the boundary layer thickens in the downstream direction. An independent relation for the wall shear stress can be obtained from Newton's law for viscosity, which ties the shear to the velocity gradient at the surface. One has

$$\tau_w = \mu \left.\frac{\mathrm{d}u}{\mathrm{d}y}\right|_{y=0} = \mu \frac{U_\infty}{\delta} F_0; \quad F_0 = \left.\frac{\mathrm{d}F}{\mathrm{d}\eta}\right|_{\eta=0}. \tag{5}$$

Here too, the parameter F_0 is determined entirely by the assumed functional form of the velocity profile. Equating the shear stress obtained from Eq. (2) with that from the viscous definition found in Eq. (5) produces a compact relation for the boundary-layer thickness in the streamwise direction [6],

$$\delta(x) = \frac{a}{\sqrt{Re_x}} x; \quad a = \sqrt{\frac{2F_0}{\theta^*}} \quad \text{and} \quad Re_x = \sqrt{\frac{\rho U_\infty x}{\mu}}. \tag{6}$$

A further quantity of interest consists of the skin friction coefficient, C_f. By replacing the shear stress at the wall, τ_w, with the expression derived from Eq. (5), the coefficient of friction can be defined in terms of the Reynolds number and non-dimensional parameters. One gets

$$C_f(x) = \frac{\tau_w}{\frac{1}{2}\rho U_\infty^2} = \frac{b}{\sqrt{Re_x}}; \quad b = \sqrt{2F_0\theta^*}. \tag{7}$$

Within the von Kármán framework, the influence of viscosity and momentum transport is contained entirely in the integral quantities associated with the assumed velocity distribution, such that the solution reduces to determining the profile-dependent constants a and b. These values provide the baseline for comparison with those obtained from Volkov's refined framework [9].

C. Volkov's Refined Approach

As described by Pitts and Griggs [9], Volkov's refinement addresses perceived limitations underlying the classical KP approach, particularly, the sensitivity of wall shear stress calculations to the assumed velocity profile [10]. The method begins with an integral form of the momentum equation originally suggested by Prandtl [11]:

$$\frac{\mathrm{d}}{\mathrm{d}x}\int_0^{\delta} u(U_\infty - u)\,\mathrm{d}y + \frac{\mathrm{d}U_\infty}{\mathrm{d}x}\int_0^{\delta}(U_\infty - u)\,\mathrm{d}y = \nu\left.\frac{\mathrm{d}u}{\mathrm{d}y}\right|_{y=0}. \tag{8}$$

Volkov notes that while the left-hand side of Eq. (8) remains relatively insensitive to errors in the assumed velocity profile, the right-hand side, which involves the derivative of an unknown function at the wall, can be highly sensitive. To address this, he introduces a refinement based on the differential forms of the boundary-layer continuity and momentum equations. Volkov [10] starts with

$$\frac{\partial u}{\partial x} + \frac{\partial v}{\partial y} = 0 \qquad \text{and} \qquad \nu\frac{\partial^2 u}{\partial y^2} = u\frac{\partial u}{\partial x} + v\frac{\partial u}{\partial y} - U_\infty\frac{\mathrm{d}U_\infty}{\mathrm{d}x}. \tag{9}$$

A single integration of these equations (after multiplying through by $\mathrm{d}y$) yields a combined relation of the form

$$\nu\frac{\partial u}{\partial y} - \nu\left.\frac{\partial u}{\partial y}\right|_{y=0} = \frac{\partial}{\partial x}\int_0^{y} u^2\,\mathrm{d}y - u\frac{\partial}{\partial x}\int_0^{y} u\,\mathrm{d}y - U_\infty\frac{\mathrm{d}U_\infty}{\mathrm{d}x}y. \tag{10}$$

A subsequent double integration is performed in order to obtain

$$\nu u - \nu y\left.\frac{\partial u}{\partial y}\right|_{y=0} = \int_0^{y}\frac{\partial}{\partial x}\left(\int_0^{y} u^2\,\mathrm{d}y\right)\mathrm{d}y - \int_0^{y} u\frac{\partial}{\partial x}\left(\int_0^{y} u\,\mathrm{d}y\right)\mathrm{d}y - U_\infty\frac{\mathrm{d}U_\infty}{\mathrm{d}x}\frac{y^2}{2}. \tag{11}$$

The single integration of the differential momentum equation effectively accumulates the momentum deficit from the wall to an arbitrary location y, whereas the subsequent double integration incorporates the convective transport of momentum across the boundary layer. Evaluating Eq. (11) at the boundary-layer edge, $y = \delta(x)$, allows the wall derivative to be expressed in terms of integral quantities. Substituting this back into Eq. (10) produces a closed-form relation, namely,

$$\frac{\mathrm{d}}{\mathrm{d}x}\int_0^{\delta} u^2\,\mathrm{d}y - U_\infty\frac{\mathrm{d}}{\mathrm{d}x}\int_0^{\delta} u\,\mathrm{d}y - \frac{U_\infty}{2}\frac{\mathrm{d}U_\infty}{\mathrm{d}x}\delta = -\frac{\nu U_\infty}{\delta} - \frac{1}{\delta}\int_0^{\delta} u\frac{\partial}{\partial x}\left(\int_0^{y} u\,\mathrm{d}y\right)\mathrm{d}y + \frac{1}{\delta}\int_0^{\delta}\frac{\partial}{\partial x}\left(\int_0^{y} u^2\,\mathrm{d}y\right)\mathrm{d}y. \tag{12}$$

At this juncture, introducing the nondimensional similarity variables $F(\eta)$ and $\eta = y/\delta$ further simplifies Eq. (12). One readily arrives at an expression for the boundary-layer thickness in terms of the local Reynolds number. One gets

$$\delta(x) = \frac{A^{-1/2}}{\sqrt{Re_x}}x; \quad A = \frac{1}{2}\left[\int_0^1\left(\int_0^{\eta} F^2\,\mathrm{d}\eta\right)\mathrm{d}\eta - \int_0^1 F\left(\int_0^{\eta} F\,\mathrm{d}\eta\right)\mathrm{d}\eta + \int_0^1 F(1-F)\,\mathrm{d}\eta\right]. \tag{13}$$

The skin-friction coefficient may be directly specified using the same wall shear formulation. One collects

$$C_f = \frac{BA^{-1/2}}{\sqrt{Re_x}}; \quad B = \int_0^1 F(1-F)\,\mathrm{d}\eta = \theta^*. \tag{14}$$

Although the final scaling with Re_x remains similar to the classical KP approach, the Volkov refinement introduces profile-dependent integral coefficients that are intended to improve the accuracy of shear-stress predictions, particularly in the close vicinity of the wall.

D. Results of Hydrodynamic Analysis

Table 1 presents the nondimensional boundary-layer parameters, $\delta\sqrt{Re_x}/x$ and $C_f\sqrt{Re_x}$, computed for a laminar flat plate using several assumed velocity profiles. Specifically first-, second-, third-, and fourth-order Pohlhausen profiles, as well as the MX4 polynomial profile, are employed to evaluate the coefficients. The resulting values are compared against the exact solution of Blasius to assess the accuracy of each assumed profile in capturing both boundary-layer growth

Table 1. Boundary-layer predictions using the Kármán–Pohlhausen (KP) method and the Volkov refinement, with errors relative to the Blasius exact solution [12–14]

		Von Kármán Method		Volkov Refinement	
Order	$F(\eta)$	$\frac{\delta}{x}\sqrt{Re_x}$	$C_f\sqrt{Re_x}$	$\frac{\delta}{x}\sqrt{Re_x}$	$C_f\sqrt{Re_x}$
KP1	η	3.464	0.577	4.000	0.667
		30.7%	13.1%	20%	0.45%
KP2	$2\eta - \eta^2$	5.477	0.730	5.071	0.676
		9.54%	9.94%	1.42%	1.81%
KP3	$\frac{3}{2}\eta - \frac{1}{2}\eta^3$	4.641	0.646	4.824	0.672
		7.18%	2.71%	3.52%	1.20%
KP4	$2\eta - 2\eta^3 + \eta^4$	5.836	0.685	5.710	0.671
		16.72%	3.16%	14.2%	1.05%
MX4	$\frac{5}{3}\eta - \eta^3 + \frac{1}{3}\eta^4$	4.993	0.668	5.029	0.672
		0.14%	0.60%	0.58%	1.2%
Exact	Blasius [2]	5.0	0.664	5.0	0.664

and wall shear characteristics. For the lower-order polynomial profiles, the Volkov refinement consistently reduces prediction error relative to the traditional von Kármán formulation. This improvement is particularly pronounced in the prediction of the skin-friction coefficient relation, $C_f\sqrt{Re_x}$. For example, for the linear profile $F(\eta) = \eta$, the Volkov refinement reduces the skin-friction error from 13.1% to 0.45%, while also decreasing the boundary-layer thickness error from 30.7% to 20%. A similar trend is observed for the quadratic profile $F(\eta) = 2\eta - \eta^2$, where both thickness and wall-shear predictions exhibit measurable improvements. For the quartic Pohlhausen profile $F(\eta) = 2\eta - 2\eta^3 + \eta^4$, the refinement again improves the skin-friction estimate (from 3.16% to 1.05%) while equally reducing the disturbance thickness error (from 16.72% to 14.2%). However, the degree of improvement diminishes and the advantage of using Volkov's refinement over Kármán's approach becomes immaterial when a more accurate quartic profile is used, namely, one that more precisely approximates the Blasius solution [6].

When the classic KP approach is used in conjunction with the MX4 quartic profile, i.e., $F(\eta) = \frac{5}{3}\eta - \eta^3 + \frac{1}{3}\eta^4$, excellent agreement with the similarity solution is immediately realized, with sub-percent errors in both thickness and skin friction. In this case, Volkov's refinement does not produce a meaningful improvement in either boundary-layer thickness or skin-friction estimation. Instead, it leads to slightly larger errors relative to the Blasius baseline. These results demonstrate that when the assumed velocity profile is well constructed and closely aligned with the Blasius solution, further refinement of Kármán's method is not necessary. When paired with a proper nearfield velocity, it stands to outperform Volkov's refinement. As shown by Majdalani and Xuan [6], the improvements associated with Volkov's refinement in some cases could be attributed to Pohlhausen's polynomials exhibiting errors that not only increase near the wall but that also tend to grow rather paradoxically with successive increases in the polynomial order. Since the MX4 profile does not suffer from these limitations, its incorporation into the KP approach enables it to outperform Volkov's refinement. Clearly, the MX4 profile provides the most reliable velocity-field predictions among the polynomial approximations considered. The Volkov refinement, however, proves advantageous at improving the wall-shear representation, particularly for lower-order approximations or weakly approximated velocity profiles.

The preceding results quantify the effect of velocity-profile selection on boundary-layer growth and wall shear stress calculations. Although convective heat transfer is determined by the wall temperature gradient, the velocity field enters the energy equation through the convective transport terms and contributes to the development of the thermal boundary layer. Consequently, variations in the predicted velocity distribution and associated shear stress have a strong bearing on the resulting heat-transfer coefficients, especially when the Reynolds-transport analogy is used.

In the thermal analysis, a distinct thermal boundary-layer thickness, δ_T, may be derived for a prescribed nearfield velocity. The ratio, δ_T/δ, can be expressed in terms of the Prandtl number, which enables us to couple the hydrodynamic and thermal problems [1]. The following section applies both the classical formulation and the Volkov refinement to the integral energy equation in order to assess their ability to predict the Nusselt number.

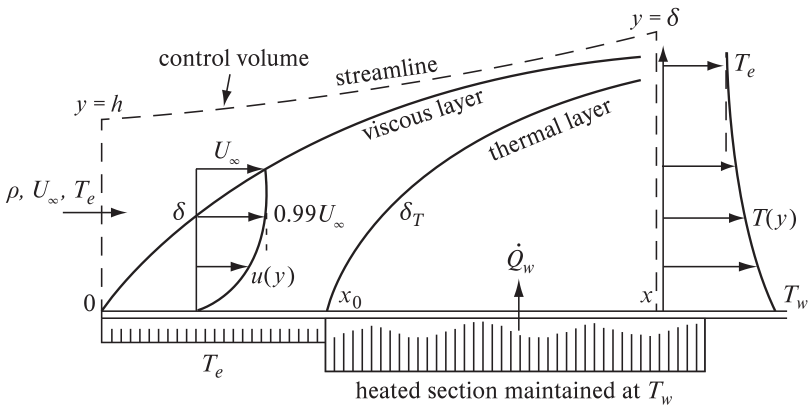

Fig. 2. Control volume used in the thermal analysis of the incompressible flow motion over a flat plate.

III. Thermal Analysis

The thermal field associated with steady, incompressible flow over an isothermal surface is now undertaken using an integral formulation of the energy equation. The classical momentum–integral framework is first applied to establish a relation between the Prandtl number and the ratio of thermal to viscous boundary-layer thickness, $\xi \equiv \delta_T/\delta$. Two regimes are considered: thin thermal layers (ξ<1) and thick thermal layers (ξ>1). This ratio ξ quantifies the competing effects of thermal and viscous momentum diffusion. The analysis is then extended using an approach inspired by Volkov's refinement to the hydrodynamic solution. In both formulations, the resulting expressions are in expressed terms of $Pr(\xi)$, which is subsequently used to compute the average Nusselt number, $\overline{Nu}_L$, thus allowing for direct comparisons to be undertaken between the classical KP and Volkov-adapted approaches.

A. Flat-Plate Configuration

As shown in Fig. 2, the plate is maintained at a constant temperature, $T_w > T_e$, with a heat flux, $\dot{Q}_w$, into the fluid. The thermal boundary layer, δ_T, represents the distance from the wall to where the fluid temperature approaches the freestream value, T_e. To facilitate the integral formulation, the temperature field is normalized using

$$F_T = \frac{T - T_w}{T_e - T_w}. \tag{15}$$

This reduction allows F_T to vanish at the wall and to reach unity in the freestream. The ratio of thermal to viscous boundary layers, ξ, captures the coupling of the momentum and thermal fields. For ξ<1, the thermal boundary layer remains embedded within the viscous region and heat transfer becomes strongly affected by the near-wall gradient. For ξ>1, the thermal layer extends beyond the viscous region into a uniform freestream velocity. In this case, the integral domain extends into the farfield where shearing effects become absent.

B. The Classical Approach

The integral form of the energy equation can be written for steady incompressible flow [1]:

$$\frac{\mathrm{d}}{\mathrm{d}x}\int_0^\infty u(T - T_\infty)\,\mathrm{d}y = -\alpha\left.\frac{\partial T}{\partial y}\right|_{y=0}. \tag{16}$$

In the above, α denotes the thermal diffusivity, which quantifies the competing effects of convective energy transport within the boundary layer and conduction at the wall. Using an assumed temperature profile, the integral equation can be expressed in terms of ξ. Prior to evaluating the integral expressions, however, it may be useful to consider the expected limiting behavior. For large Prandtl numbers, thermal diffusion becomes weak relative to momentum diffusion and the thermal layer remains embedded within the viscous region. Conversely, for small Prandtl numbers, thermal diffusion dominates and the thermal layer extends beyond the viscous layer. The integral formulation can accommodate both limits through the intrinsic dependence of Pr on ξ. Two cases arise, as detailed below.

1. Case 1: ξ<1

For thin thermal sublayers within the viscous layer, the energy equation can be reduced. One can put

$$\frac{\mathrm{d}}{\mathrm{d}x}\int_0^{\delta_T} F(F-F_T)\,\mathrm{d}y = \frac{\alpha}{U_\infty}\left.\frac{\partial F_T}{\partial y}\right|_{y=0}. \tag{17}$$

In this regime, heat transfer remains tightly coupled to the velocity profile. The left-hand side of Eq. (17) quantifies the convective accumulation of thermal energy, while the right-hand side represents conduction at the wall.

2. Case 2: ξ>1

For a thick thermal layer that envelopes the viscous layer, the energy equation becomes

$$\int_0^{\delta}\frac{\partial}{\partial x}[F(1-F_T)]\,\mathrm{d}y - \int_{\delta}^{\delta_T}\frac{\partial F_T}{\partial x}\,\mathrm{d}y = \frac{\alpha}{U_\infty}\left.\frac{\partial F_T}{\partial y}\right|_{y=0}. \tag{18}$$

Here, the thermal layer partially lies in a region of nearly uniform velocity. Splitting the integral into the viscous and outer regions enables us to properly account for the different factors.

3. Average Nusselt Number

Evaluation of Eqs. (17) and (18) yields the functional relationship, $Pr^{-1} \equiv g(\xi)$. The functional form, g(ξ), encapsulates the effect of the assumed profiles on the relative thickness of the thermal and velocity layers. The average Nusselt number, which quantifies convective heat transfer, may be determined from

$$\overline{Nu}_L = \frac{\bar{h}L}{k}; \qquad \bar{h} = \frac{1}{L}\int_0^L \frac{k}{\xi\delta}\left.\frac{\partial F_T}{\partial \eta_t}\right|_{y=0}\mathrm{d}x. \tag{19}$$

As usual, by evaluating the convective heat transfer coefficient and simplifying, one gets

$$\overline{Nu}_L = \frac{c}{\xi(Pr)}\sqrt{Re_L}, \tag{20}$$

where c can be specified by the wall-temperature gradient and the assumed boundary-layer profile. This formulation helps to ascertain that the average heat transfer is prescribed in large part by the relationship between the Prandtl number and the thermal-to-viscous boundary-layer ratio ξ. As such, the accuracy of the integral method can be seen to hinge on the fidelity with which the assumed profiles reproduce the correct Pr-ξ dependence. Moreover, in compliance with the Reynolds transport analogy, the derivative of δ_T may be evaluated assuming that variations in the thermal layer mirror those of the viscous layer. The boundary-layer thickness that we insert into Eq. (19) to simplify to Eq. (20) corresponds to the tabulated value for von Kármán's method in Table 1.

C. Approach Adapted From Volkov's Methods

In addition to the classical KP approach, an alternative formulation can be obtained by mirroring Volkov's manipulation of Eq. (8) by double integrating Eq. (16). As before, the solution can be divided into two regimes based on the thermal-to-viscous boundary-layer ratio, ξ. The derivation parallels the viscous-layer analysis by applying double integration to the energy equation with assumed temperature profiles that mimic their viscous counterparts. We hence arrive at an integral expression that is capable of deducing the Prandtl number dependence on ξ.

The motivation for adapting Volkov's refinement lies in its improved representation of the viscous boundary-layer structure through higher-order integral constraints. Because heat transfer in the ξ<1 regime is strongly tied to the velocity gradient, improvements in the hydrodynamic solution are expected to propagate directly into the thermal formulation. Here too, two cases are considered consecutively.

1. Case 1: ξ<1

For thin thermal sublayers contained within the viscous layer, double integration of the energy equation yields,

$$\alpha\left.\frac{\partial T}{\partial y}\right|_{y=0} = \frac{\alpha(T_e-T_w)}{\delta_T} - \frac{1}{\delta_T}\left[\int_0^{\delta_T}\left(\frac{\partial}{\partial x}\int_0^y (uT)\,\mathrm{d}y\right)\mathrm{d}y - \int_0^{\delta_T} T\left(\frac{\partial}{\partial x}\int_0^y u\,\mathrm{d}y\right)\mathrm{d}y\right]. \tag{21}$$

The derivative term shown in Eq. (21) can be substituted back into Eq. (16) to obtain:

$$\frac{\alpha}{\delta_T U_\infty} = \frac{\mathrm{d}}{\mathrm{d}x}\int_0^{\delta_T} F(1-F_T)\,\mathrm{d}y + \frac{1}{\delta_T}\left[\int_0^{\delta_T}\left(\frac{\partial}{\partial x}\int_0^y FF_T\,\mathrm{d}y\right)\mathrm{d}y - \int_0^{\delta_T} F_T\left(\frac{\partial}{\partial x}\int_0^y F\,\mathrm{d}y\right)\mathrm{d}y\right]. \tag{22}$$

2. Case 2: ξ>1

For thick thermal layers extending beyond the viscous sublayer, the energy equation may be expressed as

$$\int_0^{\delta}\frac{\partial}{\partial x}\left[u(T-T_e)\right]\mathrm{d}y + U_\infty\int_{\delta}^{\delta_T}\frac{\partial T}{\partial x}\,\mathrm{d}y = -\alpha\left.\frac{\partial T}{\partial y}\right|_{y=0}. \tag{23}$$

Again, double integration renders

$$\alpha\left.\frac{\partial F_T}{\partial y}\right|_{y=0} = \frac{\alpha(T_\delta - T_e)}{\delta} - \frac{1}{\delta}\left\{\int_0^{\delta}\left[\int_0^y u\left(\frac{\partial T}{\partial x}\right)\mathrm{d}y\right]\mathrm{d}y - \int_0^{\delta}\left[T\int_0^y\left(\frac{\partial u}{\partial x}\right)\mathrm{d}y\right]\mathrm{d}y + \int_0^{\delta}\left[T\left(\frac{\partial u}{\partial x}\right)\mathrm{d}y\right]\mathrm{d}y\right\}. \tag{24}$$

Equation (24) can be inserted into the wall derivative expression from Eq. (23) to produce

$$\begin{aligned}\frac{\alpha}{U_\infty}F_T\delta = &\int_0^{\delta}\left(\int_0^y\frac{\partial}{\partial x}(FF_T)\,\mathrm{d}y\right)\mathrm{d}y - \int_0^{\delta}\left(F_T\int_0^y\frac{\partial F}{\partial x}\,\mathrm{d}y\right)\mathrm{d}y\\ &+\delta\left[\int_0^{\delta}\frac{\partial F}{\partial x}\,\mathrm{d}y - \int_0^{\delta}\frac{\partial}{\partial x}(FF_T)\,\mathrm{d}y - \int_{\delta}^{\delta_T}\frac{\partial F_T}{\partial x}\,\mathrm{d}y\right].\end{aligned} \tag{25}$$

This case accounts for a thermal boundary layer that extends beyond the viscous sub-layer.

3. Average Nusselt Number

The average Nusselt number can be evaluated analogously using Eq. (19), with minor modifications to account for the refined profile. The temperature derivative $\partial T/\partial y$ can be extracted from either Eq. (21) or Eq. (23), depending on the regime under consideration. In this process, one may use the viscous boundary-layer coefficient in Table 1 corresponding to Volkov's refinement. Collectively, the classical and adapted formulations provide complementary perspectives on laminar flat-plate heat transfer. The classical approach emphasizes analytical simplicity and clear scaling behavior, whereas the Volkov-inspired refinement improves structural consistency with the viscous solution. Naturally, side-by-side comparisons of the resulting average Nusselt-number predictions against the exact similarity solution will allow for a quantitative assessment of the trade-off between analytical tractability and predictive accuracy.

D. Results of Thermal Analysis

Application of the integral energy formulation yields closed-form relations linking the Prandtl number to the thermal boundary-layer ratio. For each assumed profile, the resulting thermal relations are written as $\mathrm{Pr}^{-1} = g(\xi)$. Since the formulation depends on whether thermal or momentum diffusion dominates, the relation is separated into two different expressions. For the reader's convenience, the resulting expressions for the KP integral formulation are summarized in Table 2, whereas the corresponding relations obtained using the adapted Volkov formulation are presented in Table 3.

For the KP solution in the thin-layer regime, the Prandtl number shows an explicit dependence on polynomial powers of ξ all the way to the sixth order for higher-order profiles. This may be attributed to the initial dependence on polynomial viscous and thermal profiles. In the thick-layer regime, however, where the thermal layer encloses the viscous layer, the dependence becomes more complex. We arrive at an inverse ξ relationship that takes advantage of diminishing values of ξ^{-n} at higher powers of n.

The adapted approach seems to preserve the polynomial structure for thin layers but modifies the coefficients and higher-order contributions to better capture the energy distribution within the thermal boundary layer. In the thick-layer regime, the expressions also involve mixed powers of ξ. In practice, the Prandtl-number relations presented in Tables 2 and 3 enable us to fully characterize the coupling between the thermal and viscous boundary layers across both thin and thick thermal regimes. These relations are essential for determining the thermal boundary-layer thickness ratio,

Table 2. Expressions for Pr^{-1} using the classical KP approach given $\xi < 1$ and $\xi > 1$

	Classical KP Approach	
$F(\eta)$	$\xi < 1$	$\xi > 1$
η	ξ^3	$3\xi^2 - 3\xi + 1$
$2\eta - \eta^2$	$\frac{5}{4}\xi^3 - \frac{1}{4}\xi^4$	$\frac{5}{2}\xi^2 - \frac{5}{2}\xi + \frac{5}{4} - \frac{1}{4}\xi^{-1}$
$\frac{3}{2}\eta - \frac{1}{2}\eta^3$	$\frac{14}{13}\xi^3 - \frac{1}{13}\xi^5$	$\frac{35}{13}\xi^2 - \frac{35}{13}\xi + \frac{14}{13} - \frac{1}{13}\xi^{-2}$
$2\eta - 2\eta^3 + \eta^4$	$\frac{42}{37}\xi^3 - \frac{27}{148}\xi^5 + \frac{7}{148}\xi^6$	$\frac{189}{74}\xi^2 - \frac{189}{74}\xi + \frac{42}{37} - \frac{27}{148}\xi^{-2} + \frac{7}{148}\xi^{-3}$
$\dfrac{5}{3}\eta - \eta^3 + \dfrac{1}{3}\eta^4$	$\frac{41}{37}\xi^3 - \frac{39}{292}\xi^5 + \frac{5}{197}\xi^6$	$\frac{89}{34}\xi^2 - \frac{89}{34}\xi + \frac{41}{37} - \frac{39}{292}\xi^{-2} + \frac{5}{197}\xi^{-3}$

Table 3. Expressions for Pr^{-1} using the adapted Volkov approach given $\xi < 1$ and $\xi > 1$

	Adapted Volkov Approach	
$F(\eta)$	$\xi < 1$	$\xi > 1$
η	ξ^3	$4\xi^2 - 4\xi + 1$
$2\eta - \eta^2$	$\frac{9}{7}\xi^3 - \frac{2}{7}\xi^4$	$\left(\frac{30}{7}\xi - \frac{30}{7} + \frac{3}{7}\xi^{-1} + \frac{4}{7}\xi^{-2}\right) / \left(2\xi^{-1} - \xi^{-2}\right)$
$\frac{3}{2}\eta - \frac{1}{2}\eta^3$	$\frac{12}{11}\xi^3 - \frac{1}{11}\xi^5$	$\left(\frac{48}{11}\xi - \frac{48}{11} + \frac{8}{11}\xi^{-1} + \frac{3}{11}\xi^{-3}\right) / \left(\frac{3}{2}\xi^{-1} - \frac{1}{2}\xi^{-3}\right)$
$2\eta - 2\eta^3 + \eta^4$	$\frac{900}{773}\xi^3 - \frac{175}{773}\xi^5 + \frac{48}{773}\xi^6$	$\left(\frac{3780}{773}\xi - \frac{3780}{773} - \frac{120}{773}\xi^{-1} + \frac{1785}{773}\xi^{-3} - \frac{892}{773}\xi^{-4}\right) / \left(2\xi^{-2} - 2\xi^{-3} + \xi^{-4}\right)$
$\dfrac{5}{3}\eta - \eta^3 + \dfrac{1}{3}\eta^4$	$\frac{35}{31}\xi^3 - \frac{14}{87}\xi^5 + \frac{5}{93}\xi^6$	$\left(\frac{239}{54}\xi - \frac{239}{54} + \frac{69}{125}\xi^{-1} + \frac{111}{160}\xi^{-3} - \frac{69}{281}\xi^{-4}\right) / \left(\frac{5}{3}\xi^{-2} - \xi^{-3} + \frac{1}{3}\xi^{-4}\right)$

ξ, for a given Prandtl number. Once ξ is established, the corresponding wall-temperature gradient can be evaluated according to the methodology described in Sec. III and leading to the average Nusselt number.

In the interest of brevity, results are presented in the form of $\overline{Nu}_L Re^{-1/2}$ for a range of Prandtl numbers. By explicitly incorporating the ξ-dependent coefficients derived from the classical KP and adapted Volkov approaches, these Nusselt number calculations enable us to predict the overall heat transfer coefficient while capturing the effect of thermal–momentum layer interactions. The resulting formulations also enable us to draw direct comparisons between the classical and refined approaches, showcasing how closely they match the exact predictions.

The results presented in Tables 4 and 5 show rather categorically that increasing the order of the assumed temperature profile substantially improves predictive accuracy of the average Nusselt number. Among the profiles considered, the MX4 polynomial with the KP integral formulation consistently produces the closest agreement with the exact solution. On the one hand, assuming moderate Prandtl numbers ($0.5 < Pr < 1.1$), the classical KP-MX4 predictions differ from the exact values by less than 3%; in the same range, first-, second-, and third-order Pohlhausen profiles lead to larger deviations, particularly at high Pr, where errors can exceed 10%. Even at elevated Prandtl numbers ($Pr > 7$), the KP-MX4 approach remains quite robust by maintaining deviations within 2-5%, namely, in the viscous momentum-dominated regime.

On the other hand, Volkov's adapted integral formulation offers improvements over the use of the KP approach with the traditional Pohlhausen polynomials; moreover, the adapted approach also provides measurable improvement with the MX4 profile. In some instances, it produces negligible gains or slightly increases the error relative to the classical KP approach, especially when used with higher-order Pohlhausen polynomials. These improvements are most consistent for Prandtl numbers greater than unity ($Pr > 1$), where the adapted formulation yields reliable gains in predictive accuracy. At low Prandtl numbers ($Pr = 0.1$), the adapted approach underperforms, likely due to the assumption of a constant thermal-viscous boundary-layer thickness ratio, ξ. Physically, the thermal boundary layer at lower Prandtl numbers grows more rapidly than the momentum layer, thus leading to rapid variations in ξ near the leading edge. Since the flat plate assumes that the thermal and viscous layers start at the same point, the underlying

Table 4. Comparison of $\overline{Nu}_L Re^{-1/2}$ for KP1, KP2, and KP3 profiles to Merk solutions over a range of Pr [15]

	η		$2\eta - \eta^2$		$\frac{3}{2}\eta - \frac{1}{2}\eta^3$		
Pr	Von Kármán	Volkov	Von Kármán	Volkov	Von Kármán	Volkov	Exact
0.1	0.2507	0.2483	0.2985	0.2771	0.2705	0.2688	0.2762
0.5	0.4569	0.4832	0.5652	0.5186	0.5045	0.5148	0.5182
0.6	0.4863	0.5238	0.6052	0.5569	0.5390	0.5536	0.5537
0.7	0.5124	0.5618	0.6408	0.5914	0.5697	0.5882	0.5853
0.8	0.5359	0.5980	0.6731	0.6222	0.5974	0.6193	0.6138
0.9	0.5574	0.6328	0.7028	0.6507	0.6229	0.6472	0.6400
1	0.5774	0.6667	0.7303	0.6761	0.6464	0.6719	0.6641
1.1	0.5960	0.6881	0.7560	0.6994	0.6684	0.6944	0.6868
7	1.0446	1.2755	1.4528	1.3311	1.2595	1.3009	1.2919
10	1.2439	1.4365	1.6430	1.5039	1.4204	1.4663	1.4563

Table 5. Comparison of $\overline{Nu}_L Re^{-1/2}$ for quartic and MX4 profiles to Merk solutions over a range of Pr [15]

	$2\eta - 2\eta^3 + \eta^4$		$\frac{5}{3}\eta - \eta^3 + \frac{1}{3}\eta^4$		
Pr	Von Kármán	Volkov	Von Kármán	Volkov	Exact
0.1	0.2818	0.2771	0.2748	0.2731	0.2762
0.5	0.5316	0.5212	0.5156	0.5174	0.5182
0.6	0.5689	0.5580	0.5513	0.5554	0.5537
0.7	0.6021	0.5906	0.5832	0.5893	0.5853
0.8	0.6322	0.6198	0.6119	0.6199	0.6138
0.9	0.6598	0.6463	0.6384	0.6475	0.6400
1	0.6854	0.6707	0.6628	0.6631	0.6641
1.1	0.7093	0.6934	0.6921	0.6864	0.6868
7	1.3511	1.3067	1.3104	1.3043	1.2919
10	1.5255	1.4735	1.4789	1.4715	1.4563

abrupt changes are not captured. Overall, our findings confirm that the use of the MX4 profile in concert with the classical KP approach yields the most reliable and consistently accurate estimates across all profiles considered and Prandtl number range explored.

IV. Conclusions

In this work, a systematic comparison is carried out between the classical von Kármán integral method and Volkov's refined formulation for laminar boundary layers developing over flat surfaces. In this context, both hydrodynamic and thermal characteristics are evaluated using a range of polynomial velocity and temperature profiles. The study demonstrates that the assumed nearfield velocity profile and the integral method employed exert a strong influence on the predictive accuracy of the resulting approximations for both momentum and heat transfer properties.

For the hydrodynamic problem, the traditional Pohlhausen profiles, which are recognized for their limited fidelity, benefit substantially from Volkov's refinement, particularly in the prediction of wall shear and boundary-layer thickness, especially when low-order polynomials are adopted. For example, the first-order Pohlhausen profile, when paired with Volkov's refinement, yields a striking reduction in the skin-friction error from 13% to a mere 1%. This improvement may be ascribed to Volkov's approach being more tolerant of inaccuracies stemming from the nearfield velocity approximation. However, as the assumed velocity profile more closely mirrors the Blasius solution, the incremental advantage afforded by Volkov's refinement diminishes. In fact, the MX4 polynomial achieves sub-percent errors in both skin friction and boundary-layer thickness when incorporated into the traditional von Kármán method, thereby obviating the need for further refinements. For high-order profiles, the Volkov refinement, which effectively averages out inaccuracies introduced by the nearfield velocity, offers enhancements for the standard Pohlhausen polynomials but provides no appreciable benefits to predictions based on the MX4 profile.

This behavior is mirrored in the thermal analysis, where the standard Pohlhausen profiles benefit appreciably from the adapted Volkov techniques. Nonetheless, across the entire Prandtl number range, the classical KP-MX4 approach consistently delivers the closest agreement with exact solutions. Moderate Prandtl numbers exhibit deviations below 3%, while higher Prandtl numbers remain within 2-5% error. Lower-order profiles, in contrast, produce substantially larger deviations, exceeding 10% at high Prandtl numbers. The adapted integral formulation improves predictions for typical Pohlhausen profiles but offers minimal benefit, and in some cases, a slight detriment, when paired with the MX4 profile. At Prandtl numbers of 0.1, the adapted approach severely underperforms.

Overall, the study confirms that the careful selection of higher-order polynomial profiles proves more effective in securing accurate boundary-layer predictions than refinements to the integral formulation itself, particularly when the velocity profile already approximates the Blasius solution quite closely. The MX4 polynomial, combined with the traditional von Kármán method, consistently furnishes reliable and quantitatively accurate estimates of boundary-layer growth, wall shear, and convective heat transfer across a wide range of Prandtl numbers. Our formulations showcase the importance of suitable profile selections in boundary-layer analyses while providing an alternative framework for enhancing the accuracy of integral approximations in the presence of low-order or untested nearfield velocities.

Acknowledgments

This work is supported by the Hugh and Loeda Francis Chair of Excellence, Department of Aerospace Engineering, Auburn University.

References

[1] White, F. M. and Majdalani, J., *Viscous Fluid Flow*, McGraw-Hill, New York, 4th ed., 2021.

[2] Blasius, H., "Grenzschichten in Flüssigkeiten mit kleiner Reibung," *Journal of Applied Mathematics and Mechanics (ZAMM)*, Vol. 56, 1908, pp. 1–37.

[3] von Kármán, T., "Über laminare und turbulente Reibung," *Journal of Applied Mathematics and Mechanics (ZAMM)*, Vol. 1, No. 4, 1921, pp. 233–252. doi:10.1002/zamm.19210010401.

[4] Pohlhausen, K., "Zur näherungsweisen Integration der Differentialgleichung der laminaren Grenzschicht," *Journal of Applied Mathematics and Mechanics (ZAMM)*, Vol. 1, No. 4, 1921, pp. 252–290. doi:10.1002/zamm.19210010402.

[5] Anderson, J. D., *Fundamentals of Aerodynamics*, McGraw-Hill, Princeton, NJ, 6th ed., 2017.

[6] Majdalani, J. and Xuan, L.-J., "On the Kármán Momentum Integral Approach and the Pohlhausen Paradox," *Physics of Fluids*, Vol. 32, No. 12, December 2020, pp. 123605–20. doi:10.1063/5.0036786.

[7] Al Ahmar, R. and Majdalani, J., "On the Kármán Momentum-Integral Approach and the Pohlhausen Paradox: Extension to a Cylinder in Crossflow with a Potential Farfield Motion," *Physics of Fluids*, Vol. 34, No. 6, June 2022, pp. 063107. doi:10.1063/5.0096780.

[8] Al Ahmar, R., Majdalani, J., and Sharma, G., "Improved Viscous and Thermal Boundary-Layer Formulations for a Cylinder in Crossflow Using Kármán's Momentum-Integral Approach," *International Journal of Heat and Mass Transfer*, Vol. 240, No. 5, May 2025, pp. 126474. doi:10.1016/j.ijheatmasstransfer.2024.126474.

[9] Pitts, D. R. and Griggs, E. I., "An Improvement in Approximate Integral Methods for Convective Heat Transfer," *Integral Methods in Science and Engineering*, edited by F. R. Payne, C. C. Corduneanu, A. Haji-Sheikh, and T. Huang. Hemisphere Publishing Corporation, Washington, 1986, pp. 530–540.

[10] Volkov, V. N., "A Refinement of the Kármán–Pohlhausen Integral Method in Boundary Layer Theory," *Journal of Engineering Physics*, Vol. 9, 1965, pp. 371–374. doi:10.1007/BF00833185.

[11] Prandtl, L., "Über Flüssigkeitsbewegung bei sehr kleiner Reibung," *Proceedings of the Third International Mathematical Congress Heidelberg*, 1904, NACA Technical Memo. 452.

[12] Schetz, J. A. and Bowersox, R. D. W., *Boundary Layer Analysis*, American Institute of Aeronautics and Astronautics, 2nd ed., January 2011. doi:10.2514/4.868245.

[13] Pritchard, P. J. and Mitchell, J. W., *Fox and McDonald's Introduction to Fluid Mechanics*, Wiley, Hoboken, NJ, 9th ed., 2015.

[14] Schlichting, H. and Gersten, K., *Boundary-Layer Theory*, Springer-Verlag, Berlin, 9th ed., 2017.

[15] Merk, H. J., "Rapid Calculations for Boundary-Layer Transfer Using Wedge Solutions and Asymptotic Expansions." *Journal of Fluid Mechanics*, Vol. 5, No. 3, 1959, pp. 460–480. doi:10.1017/S0022112059000313.